

# Unveiling and Bridging the Functional Perception Gap in MLLMs: Atomic Visual Alignment and Hierarchical Evaluation via PET-Bench

Zanting Ye, Xiaolong Niu, Xuanbin Wu, Xu Han, Shengyuan Liu, Jing Hao, Zhihao Peng, Hao Sun, Jieqin Lv, Fanghu Wang, Yanchao Huang, Hubing Wu, Yixuan Yuan, *Senior member, IEEE*, Habib Zaidi, *Fellow, IEEE*, Arman Rahmim, *Senior member, IEEE*, Yefeng Zheng, *Fellow, IEEE*, and Lijun Lu

arXiv:2601.02737v1 [cs.CV] 6 Jan 2026

**Abstract**—While Multimodal Large Language Models (MLLMs) have demonstrated remarkable proficiency in tasks such as abnormality detection and report generation for anatomical modalities, their capability in functional imaging remains largely unexplored. In this work, we identify and quantify a fundamental functional perception gap: the inability of current vision encoders to decode functional tracer biodistribution independent of morphological priors. Identifying Positron Emission Tomography (PET) as the quintessential modality to investigate this disconnect, we introduce PET-Bench, the first large-scale functional imaging benchmark comprising 52,308 hierarchical QA pairs from 9,732 multi-site, multi-tracer PET studies. Extensive

This research was funded by the National Key Research and Development Program of China(2025YFE0216200), National Natural Science Foundation of China (62371221, 12326616 and 62201245), National High-end Foreign Experts Recruitment Plan (G2023030025L). (Zanting Ye and Xiaolong Niu contributed equally to this work.) (Corresponding author: Yefeng Zheng; Lijun Lu.)

Zanting Ye, Xiaolong Niu, Xuanbin Wu, Hao Sun and Lijun Lu are with the School of Biomedical Engineering, Southern Medical University, Guangzhou 510515, China (e-mail: yzt2861252880@gmail.com; longNX@163.com; xuanbinwu@foxmail.com; sunhaobme@smu.edu.cn; ljubme@gmail.com).

Xu Han is with the School of Biomedical Engineering, Shanghai Jiaotong University, Shanghai, 200240, China (e-mail: hanxv8826@gmail.com).

Shengyuan Liu, Zhihao Peng and Yixuan Yuan are with the Department of Electronic Engineering, Chinese University of Hong Kong, Hong Kong 518172, China (e-mail: liushengyuan@link.cuhk.edu.hk; zhihao.peng@cityu.edu.hk; yxyuan@ee.cuhk.edu.hk).

Jing Hao is with the Faculty of Dentistry, The University of Hong Kong, Hong Kong 999077, China (e-mail: jinghao@connect.hku.hk).

Jieqin Lv is with the Department of Nuclear Medicine, The Second Affiliated Hospital of Guangzhou University of Chinese Medicine, Guangzhou 510641, China (e-mail: jieqin811@163.com).

Fanghu Wang is with the PET Center, Department of Nuclear Medicine, Guangdong Provincial People's Hospital (Guangdong Academy of Medical Sciences), Southern Medical University, Guangzhou, China (e-mail: wfanghu1227@163.com).

Yanchao Huang and Hubing Wu are with the Department of Nuclear Medicine, Nanfang Hospital, Southern Medical University, Guangzhou 510515, China (e-mail: huangyanchao@i.smu.edu.cn; wuhby@m163.com).

Habib Zaidi is with the Division of Nuclear Medicine and Molecular Imaging, Geneva University Hospitals, CH-1211 Geneva, Switzerland (e-mail: habib.zaidi@hcuge.ch).

Arman Rahmim is with the Departments of Radiology, Physics, and Biomedical Engineering, The University of British Columbia, Vancouver, BC V6T 1Z4, Canada (e-mail: arman.rahmim@ubc.ca).

Yefeng Zheng is with the Medical Artificial Intelligence Laboratory, Westlake University, Hangzhou 310030, China (e-mail: zhengyefeng@westlake.edu.cn).

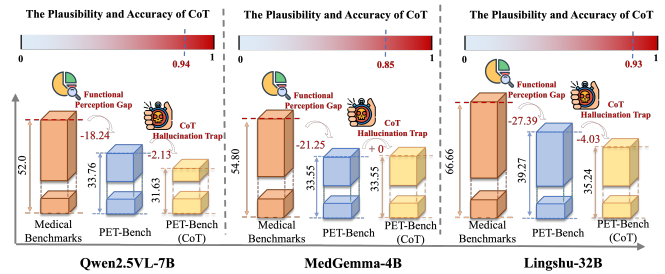


Fig. 1. Illustration of the two critical failure modes identified in MLLMs when applied to functional imaging. Functional Perception Gap: While current SOTA models achieve high performance on structural imaging benchmarks (the results from Lingshu test data), their zero-shot diagnostic accuracy on PET drops significantly. The CoT Hallucination Trap: Attempting to bridge this gap via standard CoT prompting paradoxically degrades reliability. Without domain-specific visual grounding, models generate linguistically plausible but factually ungrounded rationales, leading to high-confidence misdiagnoses.

evaluation of 19 state-of-the-art MLLMs reveals a critical safety hazard termed the Chain-of-Thought (CoT) hallucination trap. We observe that standard CoT prompting, widely considered to enhance reasoning, paradoxically decouples linguistic generation from visual evidence in PET, producing clinically fluent but factually ungrounded diagnoses. To resolve this, we propose Atomic Visual Alignment (AVA), a simple fine-tuning strategy that enforces the mastery of low-level functional perception prior to high-level diagnostic reasoning. Our results demonstrate that AVA effectively bridges the perception gap, transforming CoT from a source of hallucination into a robust inference tool and improving diagnostic accuracy by up to 14.83%. Code and data are available at <https://github.com/yezanting/PET-Bench>.

**Index Terms**—Positron Emission Tomography, Multimodal Large Language Models, Functional Imaging, Visual Question Answering, Chain-of-Thought Reasoning.

## I. INTRODUCTION

MULTIMODAL Large Language Models (MLLMs) have recently catalyzed a paradigm shift in medical artificial intelligence, demonstrating robust capabilities in interpreting anatomical modalities such as radiography, Computed Tomography (CT), and Magnetic Resonance Imaging (MRI)

[1]–[4]. By integrating advanced visual encoders with large-scale language reasoning, state-of-the-art models like GPT-5, Gemini-2.5-Pro [5] and domain-specific adaptations [1], [3] have shown remarkable success in abnormality detection and report generation. These advances have catalyzed expectations for AI-assisted diagnosis and clinical decision support in radiology [6]–[8]. Despite these advances, a critical dichotomy remains: while current methodologies excel at characterizing structural morphology (e.g., tissue density and proton relaxation), their capability to interpret functional imaging remains largely unexplored and unverified [1], [9]. This limitation is particularly acute in nuclear medicine, where diagnosis necessitates the quantification of dynamic molecular physiology and functional and molecular kinetics rather than static anatomical boundaries.

Positron Emission Tomography (PET) constitutes a fundamental metabolic and molecular imaging modality in oncology, neurology, and cardiology. Unlike CT and MRI, which provide high-frequency structural details, PET visualizes the biodistribution of radiotracers as a surrogate for underlying functional activity [10]–[12]. Interpreting these fuzzy functional and molecular heatmaps requires reasoning about tracer-specific uptake intensity, distinguishing physiological background from pathological hypermetabolism, and accounting for low-count Poisson noise. These functional semantics are intrinsically orthogonal to the edge- and texture-based features learned by standard vision encoders from natural images or structural medical datasets.

From both data coverage and model-training perspectives, PET is substantially under-represented in the current MLLM ecosystem. Existing medical MLLMs are typically derived by adapting general-domain MLLMs via instruction tuning on radiology reports, medical textbooks, and large collections of X-ray, CT, and MRI images [1], [13]. As summarized in Table I, public specifications of many medical MLLMs do not explicitly include PET as a supervised modality. Due to the relatively high cost of PET imaging, available PET resources are limited in scale, often restricted to FDG studies, and primarily target segmentation or free-text reporting without structured labels for image quality, organ-level uptake, or intermediate perceptual tasks (Table II). This structural bias motivates our hypothesis of a functional perception gap: a fundamental deficit where MLLMs, conditioned heavily on anatomical features, lose the capability to represent tracer biodistribution and voxel intensity independent of morphological priors. Consequently, these models fail to quantify dynamic metabolic and molecular processes, instead hallucinating plausible anatomical descriptions that are ungrounded in the functional signal. This hypothesis is empirically substantiated in Fig. 1, where we observe a precipitous performance drop when shifting models from structural to functional tasks, confirming that current architectures struggle to generalize beyond anatomical recognition to true functional interpretation.

Chain-of-Thought (CoT) prompting [14] has emerged as a widely adopted strategy for eliciting multi-step reasoning in large language models across mathematical, logical, and clinical decision-making tasks [15]–[17]. By encouraging models to articulate intermediate steps, CoT often enhances perfor-

mance and interpretability in purely textual and structurally grounded multimodal settings. However, most existing evidence implicitly assumes that the underlying visual perception is accurate, enabling CoT to operate on reliable intermediate representations [18], [19]. In functional imaging, this assumption is fragile. When visual grounding is weak, CoT may inadvertently amplify language priors, producing reasoning trajectories that appear clinically plausible but lack support from the image data. Whether CoT genuinely improves PET-based diagnosis or primarily increases the risk of confident but visually ungrounded explanations remains an open and clinically critical question.

In this work, we systematically characterize both the functional perception gap and the behavior of CoT-based reasoning for PET within a unified evaluation framework. We introduce PET-Bench, a multi-site, multi-tracer benchmark specifically designed for functional imaging. PET-Bench is constructed from Standardized Uptake Value (SUV)-normalized pure PET volumes without PET/CT overlays, thereby isolating functional understanding from structural priors. Guided by the cognitive workflow of nuclear medicine physicians, we structure the benchmark into a five-level hierarchy, progressing from global image perception (tracer identification and image quality assessment) to semantic grounding (organ recognition and abnormality detection), and finally to disease diagnosis. This hierarchical taxonomy allows us to pinpoint exactly where the reasoning chain breaks down: whether the model fails to see the lesion (perception gap) or fails to interpret it (reasoning deficit).

Using PET-Bench, we perform a comprehensive evaluation of a diverse panel of state-of-the-art MLLMs. We further probe diagnostic reasoning with a standardized, six-step CoT prompt mirroring clinical workflows. Our analysis reveals that current MLLMs exhibit pronounced, task-dependent deficits on PET, and that linguistically coherent CoT explanations do not guarantee correct, molecularly and grounded decisions. We term this phenomenon the CoT hallucination trap: a failure mode where the generated reasoning chain maintains high linguistic plausibility yet diverges significantly from the underlying functional signals, as illustrated in Fig. 1.

To address these limitations, we propose a simple Atomic Visual Alignment (AVA) strategy that decomposes PET interpretation into a set of clinically meaningful, atomic visual tasks used to explicitly align model representations. Concretely, we perform supervised fine-tuning on underlying visual understanding tasks in PET-Bench, enforcing that models acquire robust tracer- and organ-level metabolic and molecular perception before addressing diagnosis. All disease diagnosis cases are strictly held out for evaluation. This alignment is conceptually distinct from generic instruction tuning: it treats low- and mid-level PET perception as a prerequisite for high-level reasoning, rather than as incidental by-products of diagnostic supervision. Under this regime, CoT transitions from an unreliable intervention into a consistently beneficial reasoning mechanism for PET-based diagnosis.

In summary, this work makes three main contributions:

- We introduce PET-Bench, the first large-scale PET-focused benchmark with a five-level hierarchical VQA

TABLE I

SUMMARY OF REPRESENTATIVE MEDICAL MLLMs AND THEIR TRAINING EXPOSURE TO PET. “✓” DENOTES EXPLICIT MENTION OF PET (OR PET/CT) IN TRAINING DATA DESCRIPTIONS; “×” INDICATES ABSENCE.

Medical MLLMs	Backbone Architecture	PET
ShizhenGPT [20]	Qwen-2.5 (7B, 32B)	×
HealthGPT [21]	CLIP-L/14	×
HuaTuoGPT [13]	LLaVA-1.5	×
MedGemma [3]	Gemma 3 (4B, 27B) + SigLIP-400M	×
MedVLM-R1 [22]	Qwen2-VL-2B	×
MedDr [23]	InternVL-40B	×
Med-R1 [24]	Qwen2-VL-2B	×
Lingshu [1]	Qwen2.5-VL-7B/32B	✓

design that explicitly decomposes PET interpretation from low-level functional perception to high-level diagnosis.

- We provide a systematic evaluation of a broad range of MLLMs on PET-Bench, identifying two critical phenomena in functional imaging: a persistent functional perception gap and a CoT hallucination trap, where fluent reasoning is not a reliable proxy for correctness.
- We introduce a simple yet effective AVA, a training paradigm that effectively bridges the perception gap. Our experiments demonstrate that AVA transforms CoT from a source of hallucination into a robust inference mechanism, significantly improving diagnostic accuracy and reliability.

These contributions establish PET-Bench as a principled testbed for functional imaging, highlight the limitations of directly transferring anatomical-image MLLMs to PET, and suggest a general methodological template for developing safer, visually grounded MLLMs for PET, SPECT, and other functional modalities.

## II. RELATED WORK

### A. Multimodal Large Language Models for Medical Imaging

MLLMs have achieved impressive results on a range of anatomical imaging tasks [34]–[36]. General-purpose architectures such as CLIP [37], LLaVA [38], and Qwen-VL [39] typically serve as backbones, adapted to the medical domain via instruction tuning or lightweight fine-tuning on image-report pairs and VQA datasets [40], [41]. To enhance domain-specific reasoning, specialized models including MedGemma [3], Lingshu [1], and ShizhenGPT [20] incorporate extensive training on radiology reports, medical textbooks, and large-scale collections of X-ray, CT, and MRI volumes.

Despite these advances, a critical modality gap persists. As summarized in Table I, the supervision signal for these models is overwhelmingly dominated by structural imaging. Publicly available technical reports for leading medical MLLMs rarely list PET as an explicit training modality. A notable exception is Lingshu [1], which reports the use of PET/CT fusion data. However, reliance on fused modalities presents a confound: models may learn to extract morphological features from

the high-resolution CT component while ignoring the lower-resolution, metabolic and molecular PET signal. Consequently, the capability of current MLLMs to interpret pure functional data, where diagnosis depends on tracer uptake intensity and biodistribution rather than tissue density, remains unverified. PET-Bench addresses this by isolating the functional component, thereby rigorously testing the transferability of anatomical priors to metabolic and molecular imaging.

### B. Medical Imaging Benchmarks and PET Datasets

The evaluation of medical MLLMs has been propelled by large-scale benchmarks [25], [26], [42]–[45]. Image-text corpora such as PMC-OA [25] and ROCov2 [26] facilitate generic captioning capabilities, while VQA benchmarks like VQA-Med [42] and SLAKE [43] assess natural language reasoning over radiographs and cross-sectional anatomy [46], [47]. However, these resources provide minimal coverage of functional imaging. Existing PET-specific datasets are generally constrained by scale, tracer diversity, and task formulation. As detailed in Table II, datasets such as RIDER Lung PET-CT [27], head-neck cohorts [28], Lung-PET-CT-Dx [29], and FDG-PET-CT-Lesions [30] typically contain fewer than 1,000 studies and are restricted to single-tracer FDG imaging. Furthermore, the primary annotations in these datasets are segmentation masks or findings extraction, which support discriminative tasks but do not probe high-level reasoning. The AutoPET challenge [31] introduces dual-tracer data (FDG and PSMA) but remains focused on segmentation and quantitative volumetry. Recent efforts like PET2Rep [32] and ViMed-PET [33] target report generation; however, by evaluating holistic report quality without intermediate grounding checks, these benchmarks risk rewarding hallucinated narratives that mimic the style of radiology reports without accurately reflecting the specific image content.

### C. Chain-of-Thought (CoT) Reasoning and Visual Grounding

CoT prompting [14] has become a standard paradigm for eliciting multi-step reasoning in LLMs, effectively linearizing complex inference tasks. In the medical domain, CoT has been adapted for clinical decision support and report generation, aiming to mirror the structured workflow of human experts [48], [49]. However, the efficacy of CoT in multimodal settings is predicated on the assumption of accurate visual perception. Prior work largely assumes that if the reasoning logic is sound, the diagnostic output will be correct [18], [19]. This assumption breaks down in functional imaging, where the visual signal is subtle and physics-dependent. When an MLLM lacks the requisite features to interpret PET (the functional perception gap), CoT prompting can decouple the generated text from the image data, leading to fluent but factually incorrect explanations. We term this the CoT hallucination trap.

Our work aligns with recent efforts in hierarchical task decomposition [50] but applies it specifically to resolve this grounding failure in functional imaging. By enforcing AVA on the lower levels of the PET-Bench hierarchy, we demonstrate

TABLE II  
COMPARISON OF REPRESENTATIVE MEDICAL IMAGING DATASETS AND PET-BENCH.

Dataset	3D Volume	Tracers	Quality Annot.	Scale	Task Type
PMC-OA [25]	×	–	×	600K	Captioning
ROCOv2 [26]	×	–	×	432	Captioning
RIDER Lung [27]	✓	FDG	×	274	Findings
Head-Neck [28]	✓	FDG	×	504	Findings
Lung-PET-CT-Dx [29]	✓	FDG	×	355	Findings
FDG-PET-CT-Lesions [30]	✓	FDG	×	1,014	Segmentation
AutoPET III [31]	✓	FDG, PSMA	×	1,204	Segmentation
PET2Rep [32]	✓	FDG	×	565	Report
ViMed-PET [33]	✓	FDG	×	2,757	Report
<b>PET-Bench (Ours)</b>	<b>✓</b>	<b>FDG, PSMA, FAPI, MET</b>	<b>✓</b>	<b>9,732</b>	<b>5-Level VQA</b>

that CoT can be transformed from a source of hallucination into a robust, visually grounded diagnostic tool.

### III. PET-BENCH

To rigorously quantify the functional perception gap in current MLLMs, we introduce PET-Bench, a large-scale, multi-center benchmark explicitly designed to decouple low-level functional perception from high-level diagnostic reasoning. Fig. 2 provides an overview of PET-Bench, highlighting its key features, dataset composition, and hierarchical task structure. Given that current medical MLLMs are predominantly pre-trained on large-scale structural imaging datasets, they inherently possess strong anatomical priors. Consequently, in existing benchmarks relying on PET/CT fusion, it remains ambiguous whether successful diagnosis stems from decoding the underlying radiotracer biodistribution or merely exploiting these entrenched high-resolution CT features. Prior studies have established that pure PET imaging retains sufficient spatial information for basic organ localization and structural grounding [51], [52]. Therefore, to isolate and quantify this intrinsic functional perception capability, PET-Bench explicitly utilizes pure PET data. This design serves as a rigorous stress test, ensuring that performance metrics reflect true metabolic and molecular interpretation rather than anatomical pattern matching. To our knowledge, this constitutes the largest PET cohort to date, spanning four distinct radiotracers. Uniquely, we integrate image quality assessment as a mandatory prerequisite, grounding downstream diagnostic reliability in verified signal integrity.

#### A. Data Curation and SUV Normalization

PET-Bench aggregates 52,308 expert-curated question-answer pairs derived from 9,732 whole/total-body PET studies. Data were sourced from eight clinical centers across Asia and Europe, incorporating both public repositories (AutoPET III [31], Ultra-low Dose PET [53]) and four proprietary in-house cohorts. A distinguishing feature of our benchmark is the inclusion of data from Whole-Body PET/CT and state-of-the-art Total-Body PET/CT systems. The data acquisition covers a wide spectrum of image qualities, ranging from high-statistics clinical standard scans to simulated ultra-low-dose reconstructions. Detailed information on data sources and annotation protocols is available in Table III and Appendix A.

Raw PET data represent radioactivity concentration  $C_{raw} \in \mathbb{R}^{H \times W \times D}$  (Bq/mL), which is subject to high inter-scanner

variance due to differing acquisition protocols. To mitigate distribution shifts in the input space of the MLLM, we project all volumes onto a physiologically standardized manifold using the SUV. Let  $A_{inj}$  denote the injected dose (Bq) at time  $t_{inj}$ , and  $t_{scan}$  be the acquisition start time. The SUV-normalized volume SUV is derived as:

$$SUV = \frac{C_{raw} \cdot W}{A_{inj} \cdot e^{-\lambda(t_{scan} - t_{inj})}}, \quad (1)$$

where  $W$  is the patient’s body weight (g),  $\lambda = \frac{\ln 2}{T_{1/2}}$  is the decay constant, and  $\Delta t = t_{scan} - t_{inj}$  represents the uptake duration.

This transformation is critical for the vision encoder  $\mathcal{E}_\phi$ . Unlike natural images where intensity implies illumination, PET intensity encodes functional uptake. SUV normalization decouples the biological signal from scanner physics, ensuring that a specific scalar value represents a consistent metabolic and molecular prior across the entire dataset, thereby stabilizing the learning of the embedding space. Additionally, images were standardized to  $512 \times 512$ . Reflecting the epidemiological reality that PET is reserved for high-probability diagnostic workups rather than routine screening, the Level 5 Disease Diagnosis data consists primarily of positive cases.

#### B. Hierarchical Task Taxonomy

We structure PET-Bench not as a flat collection of VQA pairs, but as a five-level hierarchy  $\mathcal{H} = \{L_1, \dots, L_5\}$ . This taxonomy mirrors the cognitive workflow of nuclear medicine physicians and establishes a dependency chain where higher-level reasoning relies on lower-level perception.

##### 1) Level 1: Tracer Identification

The model must identify the radiotracer based solely on physiological biodistribution. This tests the model’s grasp of fundamental biological contrast mechanisms.

##### 2) Level 2: Image Quality Assessment

Functional imaging is inherently limited by low photon counts and Poisson noise. Level 2 tasks evaluate the detection of non-diagnostic quality, artifacts, and noise levels, which are distinct from natural image degradations.

##### 3) Level 3: Organ Recognition

In the absence of CT, organs must be localized via their metabolic and molecular signature. This level probes whether the model has internalized functional anatomy.

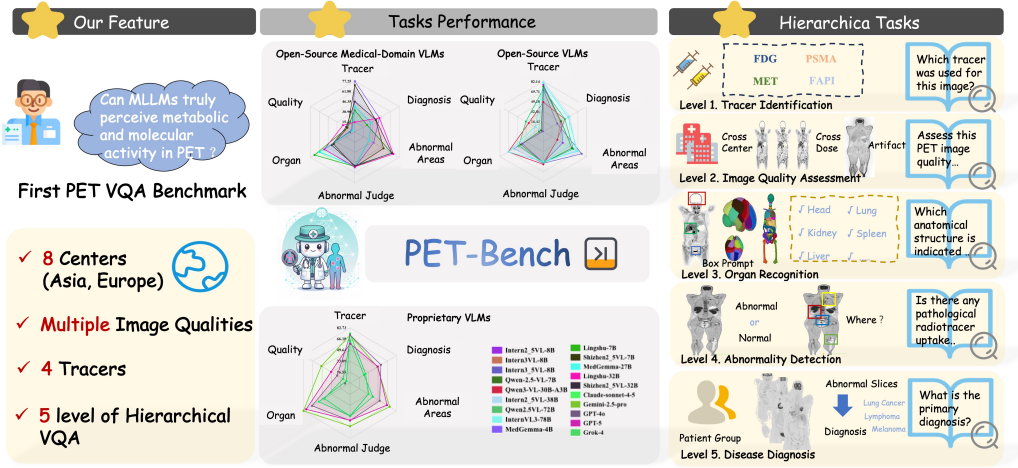


**Fig. 2.** Overview of the PET-Bench framework. PET-Bench is the first large-scale benchmark designed to evaluate functional imaging capabilities, aggregating 52,308 QA pairs from 9,732 studies across 8 international centers. Unlike generic VQA datasets, the benchmark employs a five-level hierarchical taxonomy mirroring the nuclear medicine interpretation workflow: progressing from atomic perception to lesion detection, and finally to disease diagnosis. This structure allows for explicitly decoupling perceptual failures from reasoning deficits.

**TABLE III**  
DETAILED BREAKDOWN OF THE 8 DATA CENTERS COMPRISING PET-BENCH

Center	Institution	Scanner Type	Tracer(s)	Indication	Volume
1	AutoPET / Tübingen / Munich	Various Vendors	FDG, PSMA	Multi-disease	1,611
2	German Hodgkin Study Group	Various Vendors	FDG	Lymphoma	525
3	University of Bern	Biograph Vision Quadra	FDG, PSMA	Multi-disease	1,750 <sup>†</sup>
4	Ruijin Hospital, Shanghai Jiaotong University	UIH-uEXPLORER	FDG, PSMA	Multi-disease	2,100 <sup>†</sup>
5	Nanfang Hospital, Southern Medical University	UIH-uEXPLORER	FDG, FAPI	Multi-disease	3,003 <sup>†</sup>
6		Siemens Biograph mCT	FDG	Lung Cancer	310
7	Guangdong Provincial Hospital of Chinese Medicine	Biograph Vision Quadra	MET, FDG	Multiple Myeloma	150
8	Guangdong Provincial People's Hospital	UIH-uEXPLORER	FDG, PSMA	Multi-disease	283

<sup>†</sup> Includes multi-dose reconstructions to simulate varying image qualities.

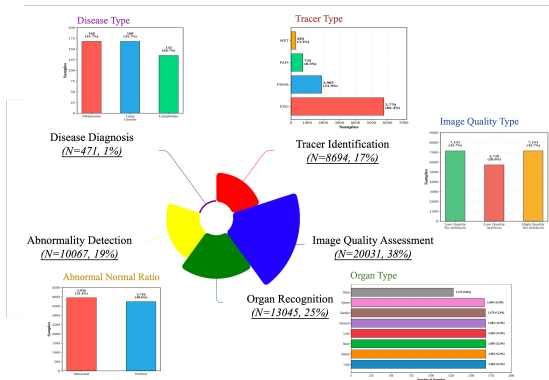


**Fig. 3.** Statistics of the PET-Bench dataset. The central sunburst chart illustrates the sample volume across the five hierarchical tasks, while outer plots detail class-wise breakdowns. The distribution reflects a deliberate design choice: large-scale data is utilized for low-level perceptual tasks to ensure robust feature learning, whereas the high-level disease diagnosis task ( $N = 471$ ) prioritizes label precision, incorporating only cases with biopsy-verified or clinically definitive outcomes.

#### 4) Level 4: Abnormality Detection

This level assesses the detection and coarse localization of hyperfunctional foci. Ground truth is derived from expert annotations, requiring the model to distinguish pathological uptake from physiological background.

#### 5) Level 5: Disease Diagnosis

The apex of the hierarchy requires synthesizing findings from  $L_1$ – $L_4$  to predict the specific pathology. To approximate clinical reading, inputs at this level are sequences of coronal slices sparsified along the cranio-caudal axis, preserving the global context of the disease burden.

Detailed statistics regarding class distribution and slice selection protocols are provided in Fig. 3. Specific data selection criteria and curation procedures for each hierarchical level are documented in Appendix B and E.

## IV. METHODOLOGY

We formulate PET diagnosis as a hierarchical probabilistic inference task. In this section, we define the domain shift problem, formalize the CoT Hallucination Trap, and introduce AVA as a solution to ground diagnostic reasoning.

### A. Problem Formulation

Let  $x \in \mathbb{R}^{H \times W}$  be a PET image and  $q$  be a clinical query. An MLLM is parameterized by  $\theta$ , consisting of a vision encoder  $\mathcal{E}_\phi$  and a language decoder  $\mathcal{D}_\psi$ . The model estimates the probability of an answer  $y \in \mathcal{Y}$ :

$$P(y | x, q; \theta) = \prod_{t=1}^T P(y_t | y_{<t}, \mathcal{E}_\phi(x), q; \mathcal{D}_\psi). \quad (2)$$

Standard MLLMs are pretrained on natural RGB images ( $\mathcal{D}_{RGB}$ ) and subsequently tuned on structural medical modalities ( $\mathcal{D}_{struct}$ , e.g., CT and MRI). In these domains, semantic information is predominantly encoded in high-frequency morphological features (edges, textures and shapes), while absolute intensity variations are often treated as illumination noise to be normalized. PET semantics are intrinsically defined by the low-frequency biodistribution of tracer intensity  $I(x)$ , where voxel magnitude directly correlates with metabolic and molecular activity. We formally define the functional perception gap not merely as a domain shift, but as a feature extraction failure: specifically, the inability of  $\mathcal{E}_\phi$  to encode intensity gradients that are orthogonal to morphological boundaries. Mathematically, let  $z = \mathcal{E}_\phi(x)$ . The gap implies that for two regions  $r_1, r_2$  with identical morphology but distinct uptake (i.e.,  $x_{r_1}^{morph} \approx x_{r_2}^{morph}$  but  $x_{r_1}^{int} \neq x_{r_2}^{int}$ ), the encoder yields  $z_{r_1} \approx z_{r_2}$ , causing the decoder  $\mathcal{D}_\psi$  to hallucinate identical descriptions based on the shared anatomical prior.

CoT prompting introduces a latent reasoning variable  $r$  (the rationale), decomposing the prediction into  $P(y | r, x, q)P(r | x, q)$ . Ideally,  $r$  acts as a bridge between visual evidence and diagnosis. However, due to the functional perception gap, the conditional probability  $P(r | x, q)$  is often dominated by the language prior  $P(r | q)$  rather than the visual input  $x$ :

$$\text{Trap} : P(r | x, q) \approx P(r | q) \implies \text{Ungrounded Reasoning.} \quad (3)$$

We term this the CoT Hallucination Trap: the model generates clinically fluent but visually detached rationales, leading to high-confidence errors.

### B. Atomic Visual Alignment (AVA)

To address this, we propose AVA, which reformulates the diagnostic process by enforcing a curriculum where the model must master atomic perceptual tasks (Levels 1–4) before attempting diagnosis (Level 5).

We partition the model parameters  $\theta = \theta_{\text{frozen}} \cup \theta_{\text{train}}$ , where  $\theta_{\text{train}}$  represents low-rank adaptation (LoRA) modules injected into the attention layers. We construct a training set  $\mathcal{D}_{AVA} = \bigcup_{\ell=1}^4 \mathcal{D}^{(\ell)}$ , strictly excluding Level 5 diagnostic cases to prevent label leakage. The AVA objective function minimizes the weighted cross-entropy over the atomic tasks:

$$\mathcal{L}_{AVA}(\theta_{\text{train}}) = - \sum_{\ell=1}^4 \lambda_\ell \mathbb{E}_{(x,q,y) \sim \mathcal{D}^{(\ell)}} [\log P(y | x, q; \theta)], \quad (4)$$

where  $\lambda_\ell$  balances the contribution of each hierarchical level. By optimizing  $\mathcal{L}_{AVA}$ , we constrain the vision-language alignment manifold such that the intermediate representations required for diagnosis (tracer type, organ location and anomalies) are explicitly grounded.

The primary motivation for AVA is to constrain the CoT used at diagnosis. In most existing MLLM settings, CoT is a post-hoc, free-form explanation whose plausibility is judged qualitatively and often influenced by the final answer [18], [19]. Such unconstrained, stochastic CoT is risky in medicine, where intermediate reasoning is expected to follow a stable clinical workflow and remain grounded in the image. PET-Bench makes this workflow explicit via its five-level hierarchy, and AVA enforces that the model’s internal reasoning is

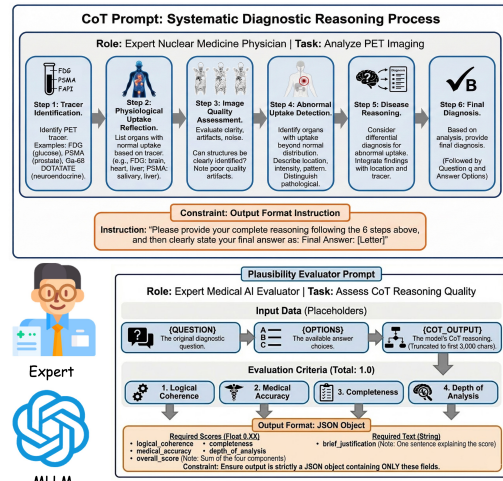


Fig. 4. Schematic workflow of the proposed CoT prompting and evaluation protocol. The six-step clinical CoT prompt instructs the model to sequentially analyze tracer type, physiological uptake, image quality, and abnormalities before concluding a diagnosis. To quantify the CoT Hallucination Trap, an auxiliary expert LLM evaluator assesses the reasoning quality across four dimensions (Logical Coherence, Medical Accuracy, Completeness and Depth) independent of the final answer correctness.

supported by verifiable atomic skills at Levels 1–4. Consequently, when CoT is enabled for diagnosis, the generated reasoning is less arbitrary and more tightly coupled to learned PET perception, enabling finer-grained analysis of where the diagnostic process succeeds or fails.

### C. Prompting Protocols and Evaluation

As shown in Fig. 4, we adopt two prompting protocols. In the zero-shot setting, the model is instructed as a medical AI assistant, receives the PET image(s) and a level-specific multiple-choice question, and must output only a single option label without explanation, probing intrinsic PET understanding. In the CoT setting, we prepend a six-step diagnostic template with the final answer constrained as “Final Answer: [LETTER]”. This mirrors nuclear medicine workflows and enables a controlled comparison between direct answers and step-by-step reasoning.

All tasks are evaluated by answer accuracy, obtained by parsing the last valid option token; responses without a valid option are counted as incorrect. To relate reasoning quality to correctness at Level 5, CoT outputs are further scored by an auxiliary LLM-based evaluator (blind to ground-truth labels) on a 0–1 scale across the four dimensions of logical coherence, medical accuracy, completeness, and depth, returning a constrained summary. The exact prompt templates used for both reasoning generation and auxiliary evaluation are provided in Appendix C.

## V. RESULTS

### A. Quantifying the Functional Perception Gap (Zero-Shot)

We first establish the baseline capabilities of current MLLMs on pure functional imaging. Fig. 5 illustrates the hierarchical tasks used for this evaluation. Table IV presents

TABLE IV

ZERO-SHOT PERFORMANCE OF 19 MLLMs ACROSS THE PET-BENCH HIERARCHY. TASKS INCLUDE TRACER IDENTIFICATION (TI), IMAGE QUALITY ASSESSMENT (IQA), ORGAN RECOGNITION (OR), ABNORMAL IDENTIFICATION (AI), ABNORMAL AREA DETECTION (AAD), AND DISEASE DIAGNOSIS (DD). **BOLD** INDICATES THE BEST PERFORMANCE, AND UNDERLINE INDICATES THE SECOND-BEST PERFORMANCE. DOMAIN-SPECIFIC MEDICAL MODELS FREQUENTLY UNDERPERFORM GENERALIST MODELS ON DIAGNOSTIC TASKS, CONFIRMING THAT ANATOMICAL PRETRAINING DOES NOT AUTOMATICALLY TRANSFER TO FUNCTIONAL IMAGING INTERPRETATION.

Model	TI	IQA	OR	AI	AAD	DD
<i>Open-Source MLLMs</i>						
InternVL2.5-8B [54]	77.21	1.36	39.60	50.90	36.83	33.55
InternVL3-8B [55]	74.21	4.02	46.50	50.60	26.81	32.48
InternVL3.5-8B [56]	68.67	0.86	55.94	51.96	<b>72.73</b>	26.33
Qwen2.5-VL-7B [39]	74.12	4.30	42.44	51.09	54.25	33.76
Qwen3-VL-30B-A3B [57]	48.31	27.82	66.43	53.78	26.60	40.98
InternVL2.5-38B [54]	<b>82.14</b>	8.20	56.49	51.10	62.20	<u>49.89</u>
Qwen2.5VL-72B [39]	70.04	33.05	46.48	50.64	57.04	40.98
InternVL3-78B [55]	<u>79.54</u>	15.67	66.43	49.17	64.61	47.13
<i>Open-Source Medical MLLMs</i>						
MedGemma-4B [3]	77.25	5.56	52.85	53.91	32.68	33.55
Lingshu-7B [1]	32.94	12.89	70.14	52.51	64.10	21.23
Shizhen2.5VL-7B [20]	71.13	12.99	36.81	53.14	49.89	36.31
MedGemma-27B [3]	38.89	4.29	61.03	52.14	25.24	28.03
Lingshu-32B [1]	14.92	20.63	53.14	52.99	67.02	39.27
Shizhen2.5VL-32B [20]	46.22	15.05	40.30	51.30	64.48	36.73
<i>Proprietary MLLMs</i>						
Claude-sonnet-4-5 [58]	74.01	6.43	55.39	48.97	32.64	27.60
Gemini-2.5-pro [59]	71.81	<b>51.02</b>	<b>82.73</b>	<b>64.23</b>	<u>70.44</u>	48.41
GPT-4o [60]	71.92	22.84	67.57	<u>55.86</u>	52.60	<b>54.78</b>
GPT-5 [61]	58.80	<u>33.79</u>	<u>78.05</u>	55.49	65.67	49.47
Grok-4 [62]	63.61	12.57	45.96	49.10	40.51	24.77

the zero-shot performance across the PET-Bench hierarchy. Three critical observations emerge regarding the transferability of current paradigms:

**1. Anatomical Training Does Not Transfer to Functional Imaging.** Contrary to the hypothesis that domain-specific models should outperform generalist models, medical MLLMs frequently underperform general-purpose architectures on diagnostic tasks. While GPT-4o achieves a diagnostic accuracy of 54.78%, Lingshu-7B and MedGemma-27B reach only 21.23% and 28.03%, respectively. This counter-intuitive result suggests that current medical adaptation protocols fail to align the vision encoder with the quantitative, intensity-based nature of PET due to their heavy reliance on anatomical data and radiology reports. The features learned from structural imaging appear orthogonal to the requirements of functional interpretation.

**2. The Bottleneck of Image Quality Assessment.** Performance on image quality assessment is uniformly poor, with a mean accuracy of 15.44% across all models. This indicates a fundamental inability to distinguish between biological signal and physics-based degradation (Poisson noise, motion artifacts). Without the capacity to assess signal integrity, downstream diagnostic reasoning rests on unstable perceptual foundations.

**3. Task-Specific Variance and Perceptual Decoupling.** While tracer identification task is relatively solvable (mean of 62.93%) due to distinct global biodistribution patterns, Diagnosis task remains challenging. Crucially, high performance

on atomic tasks does not guarantee diagnostic success in zero-shot settings. For instance, Lingshu-7B achieves competitive organ recognition (70.14%) but fails at diagnosis. This implies a perceptual decoupling: the model can localize uptake features but lacks the reasoning framework to interpret their pathological significance in a zero-shot context.

### B. The CoT Hallucination Trap

We tested the hypothesis that CoT prompting enhances reasoning in functional imaging. Table V details the impact of a six-step clinical CoT prompt on frozen base models.

**Divergence of Plausibility and Accuracy.** A critical finding is the disconnect between the fluency of the generated rationale and the correctness of the diagnosis. Across all models, CoT plausibility scores remain consistently high (0.85–0.99), yet diagnostic accuracy improvements are inconsistent. For smaller medical models, CoT either degrades performance or yields negligible gains (e.g.,  $-2.13\%$  for Qwen-2.5).

This confirms the existence of the CoT Hallucination Trap: when the visual grounding is weak (due to the perception gap), the CoT mechanism decouples from the image data. The model relies on internal language priors to generate a clinically self-consistent but factually ungrounded narrative. The high plausibility scores indicate that these hallucinations are sophisticated enough to deceive standard text-based evaluation metrics, posing a significant safety risk.

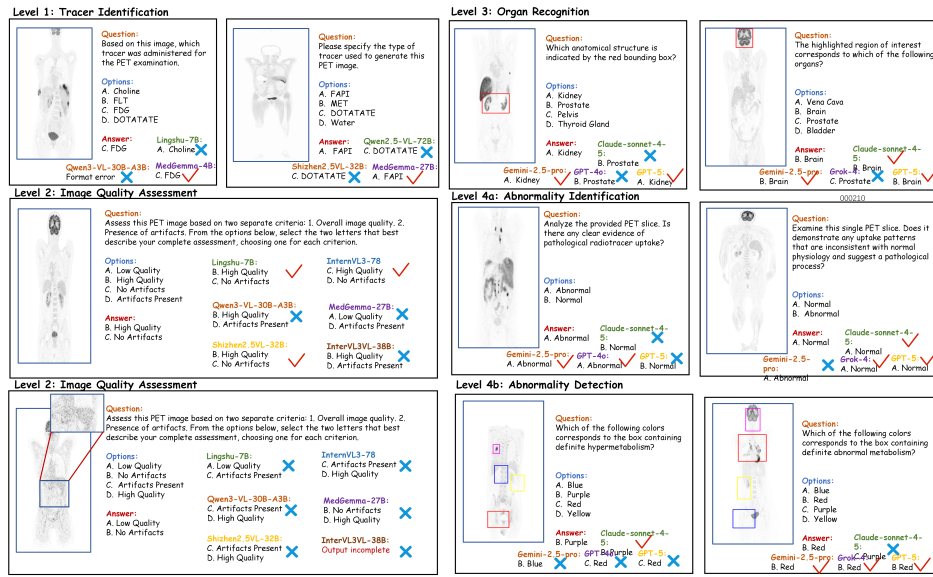


Fig. 5. Qualitative visualization of hierarchical tasks in PET-Bench (Levels 1–4). The figure displays representative failures and successes across different models. Note that generalist models often struggle with domain-specific concepts, such as distinguishing FDG from FAPI (Level 1) or identifying noise artifacts (Level 2), highlighting the necessity of the proposed atomic visual alignment.

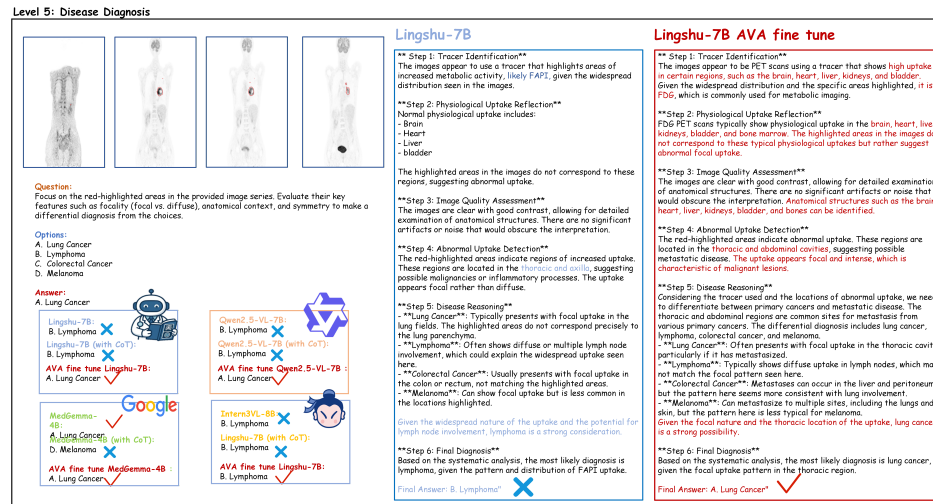


Fig. 6. Comparative case study demonstrating the efficacy of AVA. The baseline Lingshu-7B model falls into the CoT Hallucination Trap: it misidentifies the tracer distribution as lymphoma-characteristic uptake, generating a fluent but incorrect rationale. The AVA-aligned model, having been fine-tuned on atomic tasks, correctly identifies the tracer characteristics and focal thoracic uptake, successfully grounding its reasoning to diagnose Lung Cancer. This exemplifies how perceptual alignment transforms CoT from a source of noise into a robust inference mechanism.

### C. Efficacy of AVA

Table VI demonstrates the impact of our proposed AVA strategy, where models are fine-tuned exclusively on Level 1–4 atomic tasks before being evaluated on Level 5 diagnosis. The qualitative impact of this alignment is visualized in Fig. 6.

**1. Atomic Perception as a Prerequisite for Diagnosis.** Even without CoT, AVA improves direct diagnostic accuracy by margins ranging from +1.27% to +8.28%. This confirms that enforcing representations for tracer distribution and organ localization provides a better initialization for disease classification than generic instruction tuning.

**2. Resolving the Hallucination Trap.** The most significant gains occur under the AVA+CoT configuration. We specifically

focused our fine-tuning experiments on lightweight architectures, as our empirical analysis (Table V) revealed that the CoT hallucination rate is inversely correlated with model scale-making resource-constrained models particularly prone to perceptual ungrounding due to limited intrinsic capacity. Results demonstrate that AVA effectively addresses this vulnerability: unlike the frozen setting where CoT was unreliable, post-AVA CoT yields consistent and substantial improvements (e.g., +14.83% for MedGemma-4B and +15.90% for InternVL3-8B). By grounding the intermediate steps of the reasoning chain, AVA recouples the linguistic generation to the visual signal. The correlation between plausibility and accuracy is restored, transforming compact models from sources of hallucination into robust diagnostic tools.

TABLE V

THE CoT HALLUCINATION TRAP: IMPACT OF CHAIN-OF-THOUGHT PROMPTING ON FROZEN BASE MODELS.  $\Delta$  DENOTES THE ABSOLUTE ACCURACY CHANGE RELATIVE TO DIRECT ANSWERING. CRUCIALLY, WHILE CoT GENERATES HIGHLY PLAUSIBLE EXPLANATIONS, IT FREQUENTLY DEGRADES DIAGNOSTIC ACCURACY OR YIELDS MARGINAL GAINS, INDICATING A DECOUPLING BETWEEN REASONING FLUENCY AND VISUAL GROUNDING.

Model	Baseline Acc. (%)	CoT Acc. (%)	$\Delta$ (pp)	CoT Plaus. (0–1)
InternVL3-8B [55]	32.48	33.97	+1.49	0.94
Qwen2.5-VL-7B [39]	33.76	31.63	-2.13	0.94
Qwen3-VL-30B-A3B [57]	40.98	37.58	-3.40	0.95
MedGemma-4B [3]	33.55	33.55	0.00	0.85
Lingshu-7B [1]	21.23	20.60	-0.63	0.97
MedGemma-27B [3]	28.03	33.97	+5.94	0.87
Lingshu-32B [1]	39.27	35.24	-4.03	0.93
Shizhen2.5VL-32B [20]	36.73	44.80	+8.07	0.99
Claude-sonnet-4-5 [58]	27.60	37.37	+9.77	0.97
GPT-4o [60]	54.78	56.27	+1.49	0.94

TABLE VI

EFFICACY OF AVA. MODELS WERE FINE-TUNED ONLY ON LEVELS 1–4 (ATOMIC TASKS). RESULTS SHOW THAT AVA IMPROVES LEVEL-5 DIAGNOSTIC ACCURACY EVEN IN THE BASELINE SETTING, AND SIGNIFICANTLY AMPLIFIES THE BENEFIT OF CoT (AVA+CoT), VALIDATING THAT LOW-LEVEL PERCEPTUAL GROUNDING IS A PREREQUISITE FOR RELIABLE HIGH-LEVEL REASONING.

Model	Config	Acc. (%)	Gain (pp)	Plaus.
MedGemma-4B [3]	Baseline	33.55	—	—
	AVA	41.83	+8.28	—
	AVA+CoT	48.38	<b>+14.83</b>	0.89
InternVL3-8B [55]	Baseline	32.48	—	—
	AVA	37.58	+5.10	—
	AVA+CoT	48.38	<b>+15.90</b>	0.88
Qwen2.5-VL-7B [39]	Baseline	33.76	—	—
	AVA	35.03	+1.27	—
	AVA+CoT	41.40	<b>+7.64</b>	0.96
Lingshu-7B [1]	Baseline	21.23	—	—
	AVA	23.81	+2.58	—
	AVA+CoT	35.88	<b>+14.65</b>	0.95

## VI. DISCUSSIONS

### A. The Nature of the Functional Perception Gap

Our results highlight a fundamental domain shift that has been largely overlooked in medical AI: the transition from structural to functional perception. Current medical MLLMs are predominantly trained on radiology reports paired with X-ray, CT, or MRI data. In these modalities, pathology is defined by morphology. In contrast, PET pathology is defined by intensity relative to a physiological background.

The poor zero-shot performance of medical MLLMs on PET-Bench suggests that medical pretraining is not universally transferable. A model optimized for chest X-rays does not inherently understand radiotracer pharmacokinetics. The failure of these models to outperform generalist models like GPT-4o implies that without explicit exposure to the visual vocabulary of functional activity (SUV intensity, noise texture), domain-

specific medical training offers little advantage for functional imaging.

### B. The Safety Risks of Unaligned CoT

Of particular clinical significance is the identification of the CoT hallucination trap. In text-only domains, CoT is widely regarded as a technique to improve reliability. In multimodal functional imaging, we observe the opposite for unaligned models. Because the models lack the visual features to verify their own intermediate steps, the CoT process degenerates into an unconstrained text generation task.

This poses a severe safety hazard: a model might correctly identify a patient’s age and gender from the prompt, and then hallucinate a hyperfunctional lesion in the lung simply because lung cancer is a probable completion in its language model, not because it sees uptake in the image. The high plausibility scores we observed confirm that these errors are insidious, as they sound like expert opinions but lack visual grounding.

### C. Hierarchical Grounding via AVA

AVA addresses these issues not by teaching the model how to diagnose (Level 5), but by teaching it how to *see* (Levels 1–4). By conditioning the model to master tracer identification and organ-level uptake before attempting diagnosis, we impose a structural constraint on the latent space.

The success of AVA validates the hierarchical dependency of nuclear medicine interpretation. Just as a resident physician relies on mastering normal biodistribution as a prerequisite for identifying pathology, MLLMs require structured perceptual alignment that respects the causal chain of image interpretation. The substantial performance boost in the AVA+CoT setting (+14.83% for MedGemma) indicates that once the visual encoder is aligned to atomic functional concepts, the reasoning power of the LLM can be effectively leveraged.

## VII. CONCLUSION

This work introduced PET-Bench, a large-scale benchmark that exposed the functional perception gap in current Multimodal Large Language Models (MLLMs) applied to functional imaging. Our evaluation of 19 models revealed that standard pretraining on structural anatomy failed to transfer to Positron Emission Tomography (PET) interpretation, and that ungrounded Chain-of-Thought (CoT) prompting frequently led to plausible but hallucinatory reasoning. To address this, we proposed Atomic Visual Alignment (AVA), a hierarchical fine-tuning strategy that grounded diagnostic reasoning in verified low-level perceptual tasks. AVA effectively resolved the decoupling between reasoning fluency and visual fidelity. These findings underscored that reliable medical AI requires explicit alignment of visual perception prior to high-level reasoning, establishing a robust baseline for future research in functional imaging MLLMs.

## REFERENCES

- [1] W. Xu *et al.*, “Lingshu: A generalist foundation model for unified multimodal medical understanding and reasoning,” *arXiv preprint arXiv:2506.07044*, 2025.
- [2] T. Li *et al.*, “GMAI-VL & GMAI-VL-5.5 M: A large vision-language model and a comprehensive multimodal dataset towards general medical AI,” *arXiv preprint arXiv:2411.14522*, 2024.
- [3] A. Sellergren *et al.*, “MedGemma technical report,” *arXiv preprint arXiv:2507.05201*, 2025.

- [4] S. Jiang *et al.*, “HuLu-Med: A transparent generalist model towards holistic medical vision-language understanding,” *arXiv preprint arXiv:2510.08668*, 2025.
- [5] G. Comanici *et al.*, “Gemini 2.5: Pushing the frontier with advanced reasoning, multimodality, long context, and next generation agentic capabilities,” *arXiv preprint arXiv:2507.06261*, 2025.
- [6] E. Goh *et al.*, “GPT-4 assistance for improvement of physician performance on patient care tasks: A randomized controlled trial,” *Nature Medicine*, vol. 31, no. 4, pp. 1233–1238, 2025.
- [7] J. Yao *et al.*, “Multimodal GPT model for assisting thyroid nodule diagnosis and management,” *npj Digital Medicine*, vol. 8, no. 1, p. 245, 2025.
- [8] X. Liu *et al.*, “A generalist medical language model for disease diagnosis assistance,” *Nature Medicine*, vol. 31, no. 3, pp. 932–942, 2025.
- [9] Q. Zhu *et al.*, “How well do multimodal LLMs interpret CT scans? an auto-evaluation framework for analyses,” *Journal of Biomedical Informatics*, p. 104864, 2025.
- [10] L. Xue *et al.*, “[<sup>18</sup>F] FDG PET integrated with structural MRI for accurate brain age prediction,” *European Journal of Nuclear Medicine and Molecular Imaging*, vol. 51, no. 12, pp. 3617–3629, 2024.
- [11] J. Schwenck *et al.*, “Advances in PET imaging of cancer,” *Nature Reviews Cancer*, vol. 23, no. 7, pp. 474–490, 2023.
- [12] Z. Ye *et al.*, “AI-quantified <sup>11</sup>C-MET PET/CT bone marrow metabolic activity for prognostic assessment in newly diagnosed multiple myeloma,” *European Journal of Nuclear Medicine and Molecular Imaging*, pp. 1–18, 2025.
- [13] H. Zhang *et al.*, “HuatuogPT, towards taming language model to be a doctor,” in *Findings of the Association for Computational Linguistics: EMNLP 2023*, 2023, pp. 10 859–10 885.
- [14] J. Wei *et al.*, “Chain-of-thought prompting elicits reasoning in large language models,” *Advances in Neural Information Processing Systems*, vol. 35, pp. 24 824–24 837, 2022.
- [15] Y. Wang *et al.*, “V2T-CoT: From vision to text chain-of-thought for medical reasoning and diagnosis,” in *International Conference on Medical Image Computing and Computer-Assisted Intervention*. Springer, 2025, pp. 658–668.
- [16] H. Kim *et al.*, “Small language models learn enhanced reasoning skills from medical textbooks,” *npj Digital Medicine*, vol. 8, no. 1, p. 240, 2025.
- [17] K. Stechly, K. Valmeekam, and S. Kambhampati, “Chain of thoughtlessness? an analysis of CoT in planning,” *Advances in Neural Information Processing Systems*, vol. 37, pp. 29 106–29 141, 2024.
- [18] F. Barez *et al.*, “Chain-of-thought is not explainability,” *Preprint, arXiv*, p. v1, 2025.
- [19] H. Mayne *et al.*, “LLMs dont know their own decision boundaries: The unreliability of self-generated counterfactual explanations,” in *Proceedings of the 2025 Conference on Empirical Methods in Natural Language Processing*, 2025, pp. 24 172–24 197.
- [20] J. Chen *et al.*, “ShizhenGPT: Towards multimodal LLMs for traditional chinese medicine,” *arXiv preprint arXiv:2508.14706*, 2025.
- [21] T. Lin *et al.*, “HealthGPT: A medical large vision-language model for unifying comprehension and generation via heterogeneous knowledge adaptation,” *arXiv preprint arXiv:2502.09838*, 2025.
- [22] J. Pan *et al.*, “MedVLM-R1: Incentivizing medical reasoning capability of vision-language models (VLMs) via reinforcement learning,” in *International Conference on Medical Image Computing and Computer-Assisted Intervention*. Springer, 2025, pp. 337–347.
- [23] S. He *et al.*, “MedDr: Diagnosis-guided bootstrapping for large-scale medical vision-language learning,” *CoRR*, 2024.
- [24] Y. Lai *et al.*, “Med-R1: Reinforcement learning for generalizable medical reasoning in vision-language models,” *arXiv preprint arXiv:2503.13939*, 2025.
- [25] W. Lin *et al.*, “PMC-CLIP: Contrastive language-image pre-training using biomedical documents,” in *International Conference on Medical Image Computing and Computer-Assisted Intervention*. Springer, 2023, pp. 525–536.
- [26] J. Rückert *et al.*, “ROCOv2: Radiology objects in context version 2, an updated multimodal image dataset,” *Scientific Data*, vol. 11, no. 1, p. 688, 2024.
- [27] P. Li, S. Wang, T. Li *et al.*, “A large-scale CT and PET/CT dataset for lung cancer diagnosis [dataset],” *The Cancer Imaging Archive*, vol. 10, 2020.
- [28] M. Vallieres *et al.*, “Data from head-neck-PET-CT,” The Cancer Imaging Archive, 2017, available at <https://wiki.cancerimagingarchive.net/x/24pyAQ>.
- [29] P. Li, S. Wang, T. Li *et al.*, “A large-scale CT and PET/CT dataset for lung cancer diagnosis (Lung-PET-CT-Dx),” *The Cancer Imaging Archive*, 2020, [Data set]. [Online]. Available: <https://doi.org/10.7937/TCIA.2020.NNC2-0461>
- [30] S. Gatidis *et al.*, “A whole-body FDG-PET/CT dataset with manually annotated tumor lesions,” *Scientific Data*, vol. 9, no. 1, p. 601, 2022.
- [31] ———, “Results from the AutoPET challenge on fully automated lesion segmentation in oncologic PET/CT imaging,” *Nature Machine Intelligence*, vol. 6, no. 11, pp. 1396–1405, 2024.
- [32] Y. Zhang *et al.*, “PET2Rep: Towards vision-language model-driven automated radiology report generation for positron emission tomography,” *arXiv preprint arXiv:2508.04062*, 2025.
- [33] H. T. Nguyen *et al.*, “Toward a vision-language foundation model for medical data: Multimodal dataset and benchmarks for Vietnamese PET/CT report generation,” *arXiv preprint arXiv:2509.24739*, 2025.
- [34] S. Pai *et al.*, “Vision foundation models for computed tomography,” *arXiv preprint arXiv:2501.09001*, 2025.
- [35] Z. Shui *et al.*, “Large-scale and fine-grained vision-language pre-training for enhanced CT image understanding,” *arXiv preprint arXiv:2501.14548*, 2025.
- [36] H. Chen *et al.*, “Adapting vision-language models for 3D CT/MRI understanding on PMBB via slice selection and explanation analysis,” in *Proceedings of the IEEE/CVF International Conference on Computer Vision*, 2025, pp. 2273–2282.
- [37] A. Radford *et al.*, “Learning transferable visual models from natural language supervision,” in *International Conference on Machine Learning*. PMLR, 2021, pp. 8748–8763.
- [38] H. Liu, C. Li, Q. Wu *et al.*, “Visual instruction tuning,” *Advances in Neural Information Processing Systems*, vol. 36, pp. 34 892–34 916, 2023.
- [39] S. Bai *et al.*, “Qwen2.5-VL technical report,” *arXiv preprint arXiv:2502.13923*, 2025.
- [40] J. Ye and H. Tang, “Multimodal large language models for medicine: A comprehensive survey,” *arXiv preprint arXiv:2504.21051*, 2025.
- [41] H. Lin, C. Xu, and J. Qin, “Taming vision-language models for medical image analysis: A comprehensive review,” *arXiv preprint arXiv:2506.18378*, 2025.
- [42] A. B. Abacha, S. A. Hasan, V. V. Datla *et al.*, “VQA-Med: Overview of the medical visual question answering task at ImageCLEF 2019,” *CLEF (Working Notes)*, vol. 2, no. 6, pp. 1–11, 2019.
- [43] B. Liu, L.-M. Zhan, L. Xu *et al.*, “SLAKE: A semantically-labeled knowledge-enhanced dataset for medical visual question answering,” in *2021 IEEE 18th International Symposium on Biomedical Imaging (ISBI)*. IEEE, 2021, pp. 1650–1654.
- [44] J. Hao *et al.*, “OralGPT-Omni: A versatile dental multimodal large language model,” *arXiv preprint arXiv:2511.22055*, 2025.
- [45] Z. Peng, C. Wang, S. Liu *et al.*, “Omnibrainbench: A comprehensive multimodal benchmark for brain imaging analysis across multi-stage clinical tasks,” *arXiv preprint arXiv:2511.00846*, 2025.
- [46] C. Shi, R. Rezai, J. Yang *et al.*, “A survey on trustworthiness in foundation models for medical image analysis,” *arXiv preprint arXiv:2407.15851*, 2024.
- [47] R. Jin *et al.*, “FairMedFM: Fairness benchmarking for medical imaging foundation models,” *Advances in Neural Information Processing Systems*, vol. 37, pp. 111 318–111 357, 2024.
- [48] K. Le-Duc *et al.*, “S-Chain: Structured visual Chain-of-Thought for medicine,” *arXiv preprint arXiv:2510.22728*, 2025.
- [49] Z. Wu *et al.*, “Chain-of-Thought (CoT) prompting strategies for medical error detection and correction,” *arXiv preprint arXiv:2406.09103*, 2024.
- [50] T. Zhou *et al.*, “DrVD-Bench: Do vision-language models reason like human doctors in medical image diagnosis?” *arXiv preprint arXiv:2505.24173*, 2025.
- [51] Z. Ye *et al.*, “Self is the best learner: Ct-free ultra-low-dose pet organ segmentation via collaborating denoising and segmentation learning,” in *International Conference on Medical Image Computing and Computer-Assisted Intervention*. Springer, 2025, pp. 566–576.
- [52] W. Li *et al.*, “Learning ct-free attenuation-corrected total-body pet images through deep learning,” *European Radiology*, vol. 34, no. 9, pp. 5578–5587, 2024.
- [53] K. Shi, R. Guo, S. Xue *et al.*, “Ultra-low dose PET imaging challenge 2022,” in *International Conference on Medical Image Computing and Computer-Assisted Intervention*, Singapore, 2022.
- [54] Z. Chen *et al.*, “Expanding performance boundaries of open-source multimodal models with model, data, and test-time scaling,” *arXiv preprint arXiv:2412.05271*, 2024.

- [55] J. Zhu *et al.*, “InternVL3: Exploring advanced training and test-time recipes for open-source multimodal models,” *arXiv preprint arXiv:2504.10479*, 2025.
- [56] W. Wang *et al.*, “InternVL3.5: Advancing open-source multimodal models in versatility, reasoning, and efficiency,” *arXiv preprint arXiv:2508.18265*, 2025.
- [57] A. Yang *et al.*, “Qwen3 technical report,” *arXiv preprint arXiv:2505.09388*, 2025.
- [58] Anthropic, “Claude 4.5 Sonnet,” <https://www.anthropic.com/news/claude-sonnet-4-5>, 2025, accessed: 2025-12-15.
- [59] G. Team *et al.*, “Gemini: A family of highly capable multimodal models,” *arXiv preprint arXiv:2312.11805*, 2023.
- [60] OpenAI, “Hello GPT-4o,” <https://openai.com/index/hello-gpt-4o/>, 2024, accessed: 2025-12-15.
- [61] OpenAI, “GPT-5,” <https://openai.com/zh-HansCN/index/introducing-gpt-5>, 2025, accessed: 2025-12-15.
- [62] xAI, “Grok-4,” <https://x.ai/grok>, 2025, accessed: 2025-12-15.